Ordered phosphorylation events in two independent cascades of the PTEN C-tail revealed by NMR

Florence Cordier[1,2] *, Alain Chaffotte[1,2], Elouan Terrien[1,2,3], Christophe Préhaud[4,5], François-Xavier Theillet[1,2,†], Muriel Delepierre[1,2], Monique Lafon[4,5], Henri Buc[6] & Nicolas Wolff[1,2]

[1] Institut Pasteur, Unité de Résonance Magnétique Nucléaire des Biomolécules, Département de Biologie Structurale et Chimie, F-75015 Paris, France

[2] CNRS, UMR3528, F-75015 Paris, France

[3] Univ. Pierre et Marie Curie, Cellule Pasteur UPMC, rue du Dr Roux, 75015 Paris, France

[4] Institut Pasteur, Unité de Neuroimmunologie Virale, Département de Virologie, F-75015 Paris, France

[5] CNRS, URA3015, F-75015 Paris, France

[6] Institut Pasteur, F-75015 Paris, France

Supporting Information

Materials and Methods

PTEN-Ctail expression and purification.

Recombinant unlabeled and U-^{15}N/^{13}C-labeled C-terminal tail of PTEN (PTEN-Ctail, 54 residues including residues V351-V403 of human PTEN and a N-terminus non-native Met resulting from cloning) were produced as follow [1]: wild type PTEN-Ctail and mutants (S380A and S380A/T382A/T383A/S385A PTEN-Ctail) were encoded as a N-terminal Glutathione S-Transferase (GST) tagged protein in a pDEST15 expression plasmid (Gateway System, Invitrogen) and in a pGEX-6P-1 expression plasmid (GE healthcare life sciences), respectively. The vector was used to transform *Escherichia coli* BL21 (DE3) star (Invitrogen). Cells were grown in a 2.5 l bioreactor of LB medium for unlabeled PTEN-Ctail and of stable-isotopically labeled M9 minimal medium containing 1.0 g/l ^{15}NH$_4$Cl and 2.0 g/l ^{13}C-glucose as the sole nitrogen and carbon sources for U-^{15}N/^{13}C-labeled PTEN-Ctail. Protein expression was induced at OD$_{600nm}$ 0.8 – 1.0 with 1.0 mM IPTG at 30°C for 3 h. Harvested

cells were resuspended in buffer A (50 mM Tris-HCl, 150 mM NaCl, pH 7.5) with 2 mM β-mercaptoethanol and a protease inhibitor cocktail (Roche) and then disrupted in a French press. Clarified cell lysate was then loaded on a GST column (GSTrap HP, GE) equilibrated with buffer A. The tag-GST was cleaved by the TEV protease (1% M/M) directly injected on the column overnight at 4°C. The samples containing the PTEN-Ctail were pooled and concentrated to 1.0 ml and loaded onto a size exclusion column (Sephacryl S-100 HP 16/60, GE) equilibrated with buffer A. All purification steps were performed at +4°C and in presence of a protease inhibitor cocktail (Roche). Size, purity and sequence of the PTEN-Ctail samples were checked by SDS-Page, mass spectroscopy and microsequencing using Edman degradation. U-^{15}N/^{13}C-labeled PTEN-Ctail was concentrated with a Vivaspin 6 centrifugal filter device (3 000 MWCO, Sartorius). Protein concentration was estimated from its absorbance at 280 nm assuming a calculated ε_{280} of 2980 M^{-1}.cm^{-1}.

For the NMR experiment, a stock solution of U-^{15}N/^{13}C-labeled PTEN-Ctail was prepared at a concentration of 600 μM, in a solution containing 50 mM Tris-HCl pH 7.5, 150 mM NaCl, 90% H$_2$O and 10% D$_2$O.

SELDI-TOF-MS experiments.

PTEN-Ctail (unlabeled) was incubated with CK2 and GSK3β kinases, 2 mM ATP and 10 mM MgCl$_2$-containing kinase buffer. The CK2- and GSK3β-reactions were stopped at 100°C for 10 min and the samples were analyzed using the SELDI-TOF-MS technology. Several concentrations of PTEN-Ctail (from 10 to 30 μM), CK2 kinase (from 3 to 20 nM) and GSK3β kinase (30 nM) as well as times of phosphorylation reaction (from 5 min to 4 hours) were tested at 30°C and 37°C in order to set up the phosphorylation conditions for the NMR experiments. 5 μl of Gallium nitrate (50 mM) were applied twice on each spot of the immobilized metal affinity chromatography 30 (Imac 30) chemical surface (BIO-RAD) under shaking, wet air and at room temperature. Then, 5 μl of binding buffer were added on

each spot for 1 hour under the same conditions. PTEN-Ctail sample was diluted in binding buffer and 1200 fmoles of peptides were spotted on each spot from Imac 30. Samples were incubated for 60 min at room temperature under shaking. Then, the chip was washed: three times with the binding buffer, and four times in water. The samples were air-dried. 0.7 μl of α-Cyano-4-hydroxycinnamic acid (CHCA) saturated was diluted in 50% acetonitrile – 0.5% trifluoroacetic acid and was applied twice on each spot and the spots were air-dried. Spectra were generated with 7 shots at an intensity of 1600 nJ and a focus mass at 6500 Da (SELDI-TOF pcs4000 model). External mass calibration curve was performed on one spot of each array by using Human ACTH (1-24), Bovine Insulin B-chain, Human Insulin and recombinant Hirudin. Raw spectra were processed and analyzed with the Ciphergen Express data manager software version 3.0 (CE; Ciphergen Biosystems). Spectra were externally calibrated with Human ACTH (2933.5 +1H), Bovine Insulin B-chain (3495.9 + 1H), Human Insuline (5807.7 + 1H) and recombinant Hirudin (6963.5 + 1H). The baseline was established using default parameters and spectral intensities were normalized by total ion current (TIC).

In vitro CK2- and GSK3β-phosphorylation assays by NMR spectroscopy.

For the *in vitro* experiment, the pH of the NMR sample (Shigemi NMR microtubes) of U-^{15}N/^{13}C-labeled PTEN-Ctail was adjusted to 6.7, since resonance intensities of Ser and Thr residues of interest were severely weakened at pH above 6.7, due to extensive amide proton exchange with solvent.

The commercially available unlabeled CK2 kinase was purchased from Merck Millipore (Casein kinase 2α, active; MW 48.7 kDa, purity > 95%, Catalog #14-445) with a given specific activity of 1310 pmol/min/μg on a model substrate peptide. The commercially available unlabeled GSK3β kinase was purchased from Merck Millipore (GSK3β, active; MW 51 kDa, purity 97%, Catalog #14-306) with a given specific activity of 881 pmol/min/μg on a model substrate peptide. The MgCl$_2$-containing kinase

buffer was purchased from Cell Signaling Technology (Catalog #9802) and contained 25 mM Tris-HCl (pH 7.5), 5 mM β-glycerophosphate, 2 mM DTT, 0.1 mM Na_3VO_4, 10 mM $MgCl_2$.

The series of ^1H-^{15}N HSQC recorded in the time course of the CK2 or GSK3β reaction were acquired for acquisition times increasing from 6 min (at the beginning of the reaction) to 90 min (at the end). After about 120 hours of GSK3β reaction, the pH of the sample started to decrease, likely due to ATP hydrolysis, inducing overall resonance shifts in the HSQC spectra.

Preparation of human neuroblastoma cell extracts for NMR experiments.

SH-SY5Y human neuroblastoma cells were grown as described in [2]. Cells were differentiated with 10 mM db-cAMP as described by [3]. Cellular extracts were made 48 hours post drug treatment. Briefly, 10^8 cells were harvested and rinsed with PBS (Life Technologies, U.K.). The cell pellet was resuspended in 0.4 ml of lysis buffer [Complete lysis buffer (pH 7.5, Cell signaling, #9803), two tablets of complete protease inhibitor cocktail (Roche, #11697498001), two tablets of phosphatase inhibitor cocktail (Roche, phosSTOP #4906845001)], kept on ice for 15 min with gentle shaking every 2 min, then centrifuged at 13 000 g for 10 min at 4°C. The supernatant was treated with benzonase and incubated further at 4°C for 15 min. The cell lysate was centrifuged at 13 000g for 10 min at 4°C. The supernatant was aliquoted in 50 μl fractions and deep frozen in liquid nitrogen. Protein concentration (12 to 15 mg/ml) was determined by micro BCA (Pierce, USA).

Western blotting.

Cell extracts from SH-SY5Y human neuroblastoma was subjected to electrophoresis (SDS-PAGE), transferred to a PVDF membrane, and immunoblotted with CK2α Rabbit polyclonal antibody (Cell Signaling, #2656) and GSK3β rabbit monoclonal antibody (Cell signaling, #9315) using Rabbit TrueBlot®: Anti-Rabbit IgG HRP (eBioscience, #18-8816). Blots were prepared using SuperSignal

West Pico Chemiluminescent Substrate (Thermo Scientific). Exposure time was 5 minutes. Primary and secondary antibodies were diluted (1:1000 and 1:3000, respectively) in PBS (Phosphate Buffered Saline) buffer containing 2% BSA and 0.1% Tween 20.

Numerical simulation of the dynamic process of phosphorylation in the S380-S385 cluster.

In order to evaluate the dependence of the $k_{app,i}$ on the initial concentrations of substrate and enzyme, we generated simulations of the time distribution of the concentration of all species, based on the more realistic reaction scheme shown in panel A of Figure S8. According to this still simplified enzymatic mechanism, the enzyme CK2 is assumed to process each phosphorylation step through a standard minimum enzymatic reaction, that is, the reversible formation of the enzyme/substrate complex, governed by the intrinsic rate constant k_i and k_{-i}, followed by an irreversible dissociation of this complex towards the product of the reaction depending on the catalytic rate constant $k_{cat,i}$. Due to the large excess of ATP (2 mM) and its moderate consumption, the binding of this second substrate as well as the release of ADP are omitted in this scheme. According to the simple 2-step enzyme substrate reaction, the Michaelis-Menten approximation predicts a steady state for the enzyme-substrate intermediate, that is a 0 order reaction (linear time-decay of the substrate concentration) as long as the dissociation of the intermediate complex towards the product is the rate limiting step of the reaction. As the substrate is consumed, the steady state tends to end up for the benefit of a continuous succession of pseudo-first order reactions, with a minor time-dependence of the instantaneous rate constant. The duration of the steady state along the time course of the reaction depends on the value of $k_{cat,i}$ relative to the product of k_i by the substrate concentration. In the case of the reaction of PTEN-Ctail with CK2, the time distribution of our experimental data could be satisfactorily fitted to multiexponential equations for any step, which indicates a short-term steady state situation.

The commercial program VisSim 3.0 (Visual Solutions, Westford, MA) was used to simulate the time course of the concentrations of substrate and product of each reaction, S to P4, by numerical

integration of the differential equations describing the kinetic mechanism, using the 5th order Runge-Kutta method (1.08 10^6 steps; step size 0.05). Starting from our experimental conditions (initial substrate concentration $[S]_0$ of 120 µM and total enzyme concentration $[E]_0$ of 8 nM), the 12 parameters k_i, k_{-i} and $k_{cat,i}$ were manually optimized to reproduce at best the variation upon time of species A to E measured experimentally. With the rate constants k_{-i} arbitrary set to 1 s^{-1}, the following set of constants was retained (see Figure S8, panel B):

$k_1 = 0.1$ s^{-1}µM^{-1} $\qquad$ $k_{-1} = 1$ s^{-1} $\qquad$ $k_{cat,1} = 20$ s^{-1}

$k_2 = 0.035$ s^{-1}µM^{-1} $\qquad$ $k_{-2} = 1$ s^{-1} $\qquad$ $k_{cat,2} = 20$ s^{-1}

$k_3 = 0.042$ s^{-1}µM^{-1} $\qquad$ $k_{-3} = 1$ s^{-1} $\qquad$ $k_{cat,3} = 8$ s^{-1}

$k_4 = 0.03$ s^{-1}µM^{-1} $\qquad$ $k_{-4} = 1$ s^{-1} $\qquad$ $k_{cat,4} = 3$ s^{-1}

Using this set of intrinsic rate constants, we then examined the effect of changing $[S]_0$ and $[E]_0$ on the kinetics of each of the species S, P1, P2, P3 and P4. Then, from a global fitting of the time course of these species to equations (1a) to (1e) given below, we deduced the apparent rate constant $k_{app,i}$ associated to each step of substrate to product conversion, as we did with our experimental NMR data.

As shown in panel C of Figure S8, at constant $[E]_0$ (8 nM), decreasing $[S]_0$ from 120 to 50 µM results in a slight increase (about 20%) of each apparent rate constant. The ratios between apparent rate constants are independent on $[S]_0$ indicating that a change of the initial substrate concentration in the cell extracts should only have a global scaling effect on the apparent rate constants determined *in vitro*.

As shown in panel D of Figure S8, at constant $[S]_0$, increasing $[E]_0$ results in a speeding up the kinetics. The variation of the apparent rate constants with $[E]_0$ is linear, as intuitively expected, indicating that a change of the enzyme concentration has only a global scaling effect on the apparent rate constants.

Equations of the linear 5-state model

According to the linear 5-state model:

$$A \xrightarrow{\text{k}_{app,1}} B \xrightarrow{\text{k}_{app,2}} C \xrightarrow{\text{k}_{app,3}} D \xrightarrow{\text{k}_{app,4}} E,$$
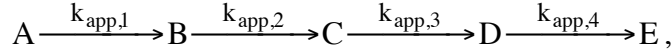
the time course of the disappearance/appearance of each phosphorylated species A to E in the S380-S385 cluster (called species A' to E' in the S361-T366 cluster) is given by the following equations:

$$A = A_0 \exp^{-\text{k}_{app,1}t} \tag{1a}$$

$$B = A_0 \left\{ \frac{-\text{k}_{app,1}}{\text{k}_{app,1} - \text{k}_{app,2}} \exp^{-\text{k}_{app,1}t} - \frac{-\text{k}_{app,1}}{\text{k}_{app,2} - \text{k}_{app,1}} \exp^{-\text{k}_{app,2}t} \right\} \tag{1b}$$

$$C = A_0 \left\{ \frac{\text{k}_{app,1}\text{k}_{app,2}}{\left(\text{k}_{app,1} - \text{k}_{app,2}\right)\left(\text{k}_{app,1} - \text{k}_{app,3}\right)} \exp^{-\text{k}_{app,1}t} + \frac{\text{k}_{app,1}\text{k}_{app,2}}{\left(\text{k}_{app,2} - \text{k}_{app,1}\right)\left(\text{k}_{app,2} - \text{k}_{app,3}\right)} \exp^{-\text{k}_{app,2}t} \right.$$
$$\left. + \frac{\text{k}_{app,1}\text{k}_{app,2}}{\left(\text{k}_{app,3} - \text{k}_{app,1}\right)\left(\text{k}_{app,3} - \text{k}_{app,2}\right)} \exp^{-\text{k}_{app,3}t} \right\} \tag{1c}$$

$$D = A_0 \text{k}_{app,1}\text{k}_{app,2}\text{k}_{app,3} \left\{ \frac{-\exp^{-\text{k}_{app,1}t}}{\left(\text{k}_{app,1} - \text{k}_{app,2}\right)\left(\text{k}_{app,1} - \text{k}_{app,3}\right)\left(\text{k}_{app,1} - \text{k}_{app,4}\right)} - \frac{\exp^{-\text{k}_{app,2}t}}{\left(\text{k}_{app,2} - \text{k}_{app,1}\right)\left(\text{k}_{app,2} - \text{k}_{app,3}\right)\left(\text{k}_{app,2} - \text{k}_{app,4}\right)} \right.$$
$$\left. - \frac{\exp^{-\text{k}_{app,3}t}}{\left(\text{k}_{app,3} - \text{k}_{app,1}\right)\left(\text{k}_{app,3} - \text{k}_{app,2}\right)\left(\text{k}_{app,3} - \text{k}_{app,4}\right)} - \frac{\exp^{-\text{k}_{app,4}t}}{\left(\text{k}_{app,4} - \text{k}_{app,1}\right)\left(\text{k}_{app,4} - \text{k}_{app,2}\right)\left(\text{k}_{app,4} - \text{k}_{app,3}\right)} \right\} \tag{1d}$$

$$E = A_0 \left\{ \frac{\text{k}_{app,2}\text{k}_{app,3}\text{k}_{app,4}}{\left(\text{k}_{app,1} - \text{k}_{app,2}\right)\left(\text{k}_{app,1} - \text{k}_{app,3}\right)\left(\text{k}_{app,1} - \text{k}_{app,4}\right)} \exp^{-\text{k}_{app,1}t} + \frac{\text{k}_{app,1}\text{k}_{app,3}\text{k}_{app,4}}{\left(\text{k}_{app,2} - \text{k}_{app,1}\right)\left(\text{k}_{app,2} - \text{k}_{app,3}\right)\left(\text{k}_{app,2} - \text{k}_{app,4}\right)} \exp^{-\text{k}_{app,2}t} \right.$$
$$\left. + \frac{\text{k}_{app,1}\text{k}_{app,2}\text{k}_{app,4}}{\left(\text{k}_{app,3} - \text{k}_{app,1}\right)\left(\text{k}_{app,3} - \text{k}_{app,2}\right)\left(\text{k}_{app,3} - \text{k}_{app,4}\right)} \exp^{-\text{k}_{app,3}t} + \frac{\text{k}_{app,1}\text{k}_{app,2}\text{k}_{app,3}}{\left(\text{k}_{app,4} - \text{k}_{app,1}\right)\left(\text{k}_{app,4} - \text{k}_{app,2}\right)\left(\text{k}_{app,4} - \text{k}_{app,3}\right)} \exp^{-\text{k}_{app,4}t} + 1 \right\} \tag{1e}$$

where A, B, C, D, E (called A', B', C', D', E' for the S361-T366 cluster) are the resonance amplitudes of residues in each species, with $A_0 = A+B+C+D+E$ and $\text{k}_{app,1}$, $\text{k}_{app,2}$, $\text{k}_{app,3}$ and $\text{k}_{app,4}$ are the apparent rate constants of the S385, S380, T383 and T382 phosphorylation events, respectively (called $\text{k'}_{app,1}$, $\text{k'}_{app,2}$, $\text{k'}_{app,3}$ and $\text{k'}_{app,4}$ for T366, S362, S361 and T363, respectively). Each apparent rate constant depends on the rates for reversible enzyme binding and for catalysis and product dissociation, and is specific for a given concentration of substrate and kinase.
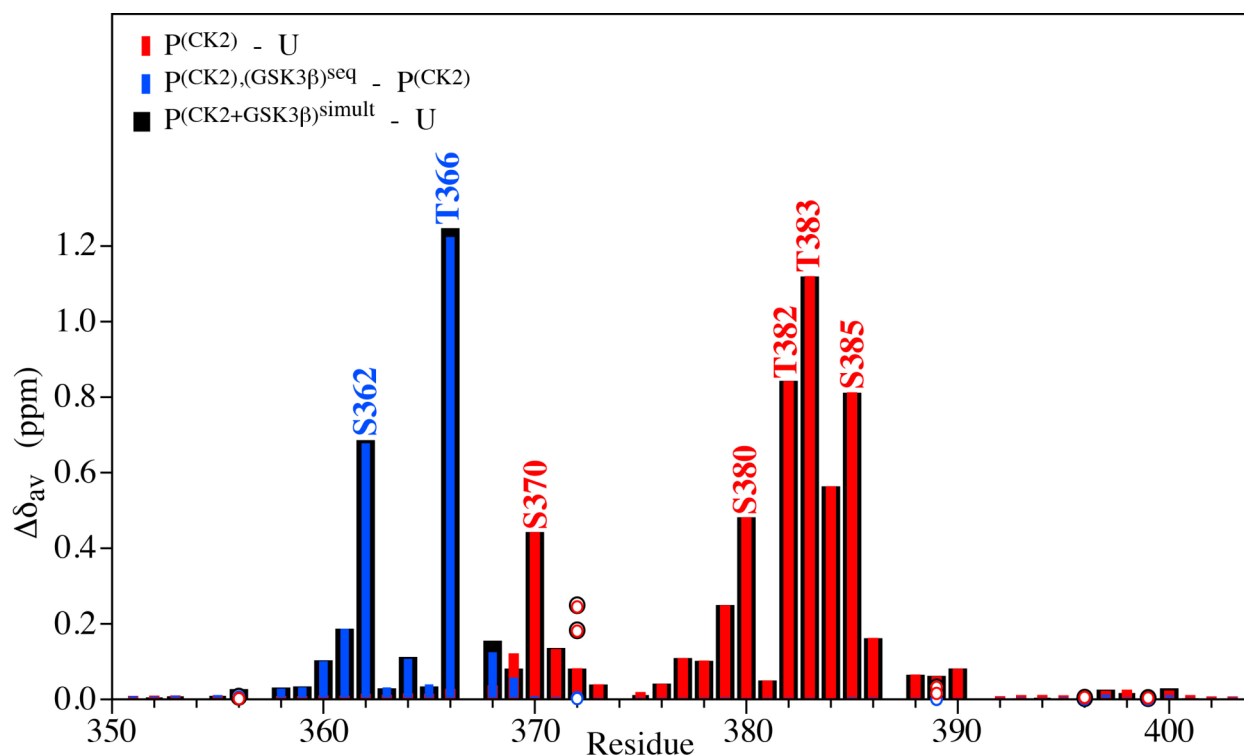
Figures

Figure S1. Phosphorylation-induced NMR chemical shift perturbations. Average (^{1}H, ^{15}N) chemical shift changes, calculated as $\Delta\delta_{av} = [(\Delta\delta_H)^2 + (\Delta\delta_N \times 0.159)^2]^{1/2}$, induced upon sequential phosphorylation by CK2 after 21 h (red, CK2-phosphorylated to unphosphorylated) and by GSK3β after 9 h (blue, sequentially CK2- and GSK3β-phosphorylated to CK2-phosphorylated) or by simultaneous phosphorylation by the two kinases (black, simultaneous CK2- and GSK3β-phosphorylated to unphosphorylated). Open circles correspond to NH2 groups of Asn and Gln residues. ^{1}H and ^{15}N chemical shifts of Ser/Thr residues phosphorylated by CK2 and GSK3β (labeled in red and blue respectively) are the most affected. Chemical shifts can be sensitive to phosphorylation-induced changes in the neighborhood of a phosphorylated residue up to n ± 5.
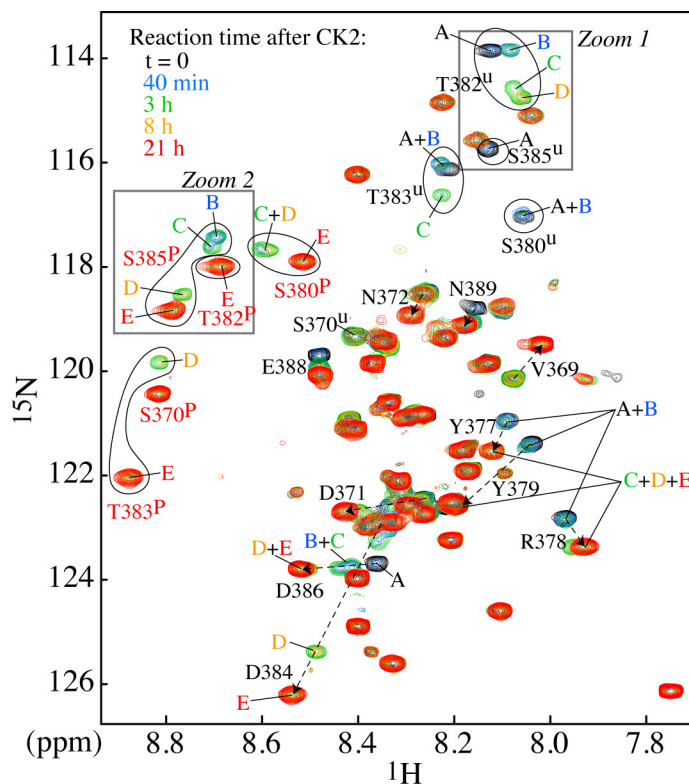
Figure S2. Superimposition of ^1H-^{15}N HSQC spectra of $^{15}N/^{13}C$-labeled PTEN-Ctail recorded in the time course of the CK2 reaction from t = 0 to 21 hours (black, blue, green, orange to red). Resonance assignment is indicated for the Ser/Thr residues and their neighbors in each phosphorylated species A to E. The two regions described in Figure 2B of the manuscript are delineated by the two boxes (zoom 1 and zoom 2).
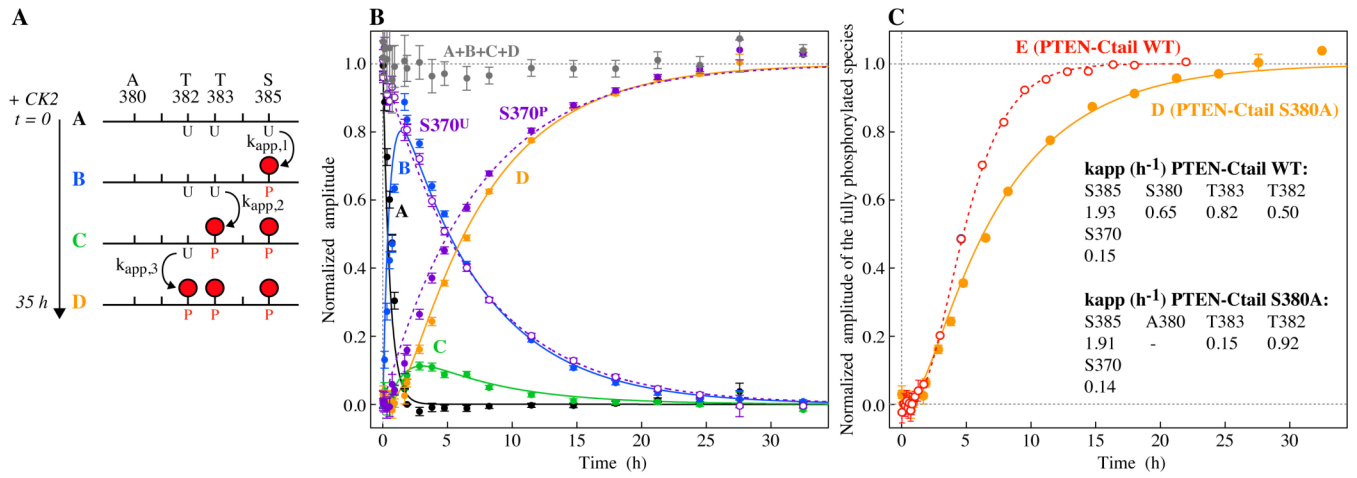
Figure S3. Comparison of the kinetics of phosphorylation in the wild type and the S380A mutant PTEN-Ctail *in vitro*. To assess to which extent the cascade of phosphorylation events is affected in the downstream pathway by point mutation of a Ser/Thr along the sequence, we performed an *in vitro* experiment on a S380A PTEN-Ctail mutant in the same conditions as for the wild type. **(A)** Definition of the phospho-forms within the T382-S385 cluster as they appear in time in the sequential reaction model (from species A to D). U or P denotes unphosphorylated or phosphorylated by CK2. **(B)** Amplitudes of the averaged normalized resonance signals for each species A to D (and their sum) are plotted as a function of the CK2 reaction time. Error bars correspond to the rms of the noise in the corresponding spectrum. The curves (solid lines) are the result of a global non-linear least square fitting of the amplitudes *A* to *D* to equations derived from the linear 3-step model (following the same rational as for the wild type 4-step model). The time course of the normalized amplitudes of S370^U and S370^P resonances (open and close violet circles) was fitted to a single exponential function (dashed lines). **(C)** Normalized amplitude of the fully phosphorylated species, E for the wild type (red) and D for the S380A mutant (orange). The delay in the appearance of the fully phosphorylated species of the mutant is clearly visible. The values of the apparent rate constants are given for the wild type (WT) and the S380A mutant.
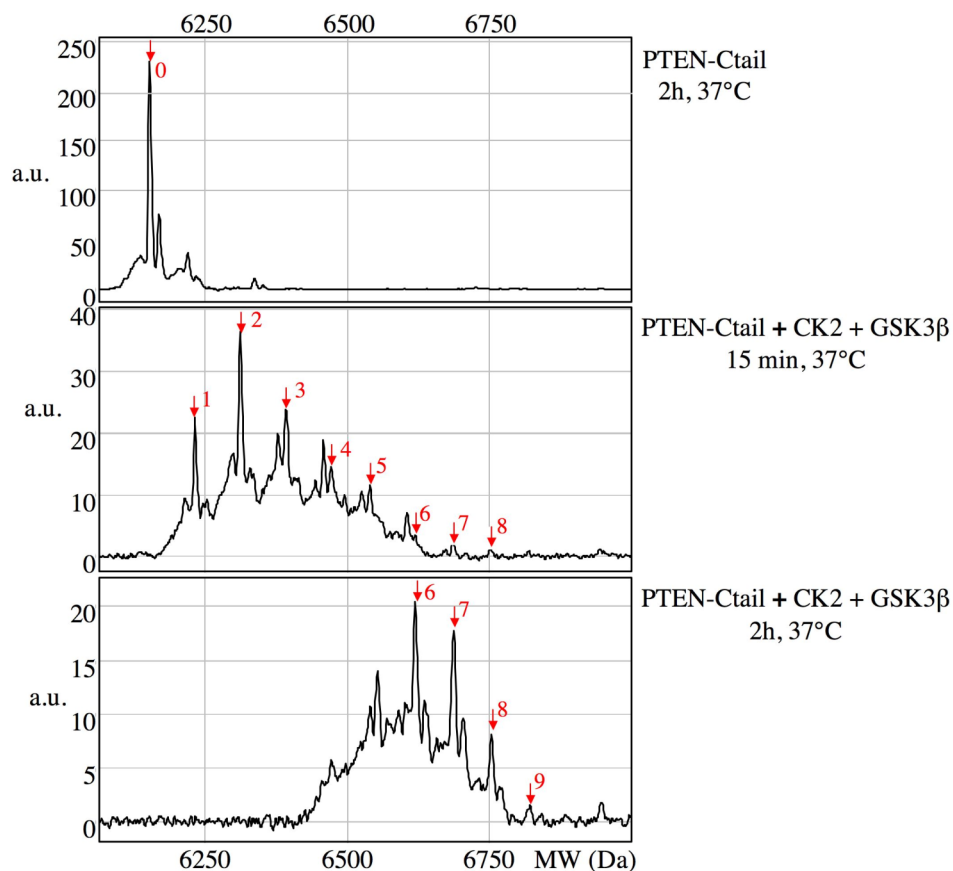
Figure S4. SELDI-TOF-mass spectrometry profiles of PTEN-Ctail phosphorylated by CK2 and GSK3β kinases. PTEN-Ctail (12 μM) was incubated with 6 nM of CK2 and 30 nM of GSK3β, 2 mM ATP and 10 mM MgCl$_2$-containing kinase buffer at 37°C. As control, PTEN-Ctail was monitored after 2 hours at 37°C in the absence of kinase (upper panel). In the presence of CK2 and GSK3β, aliquot were removed at 15 min (middle panel) and 2 hours (lower panel) after the beginning of the phosphorylation reaction. The kinase-reaction was stopped and the samples were analyzed using the SELDI-TOF-MS technology. Peaks matching the molecular weight of PTEN-Ctail and of its phosphorylated forms are indicated by arrows on the spectra. Nine phosphorylation events of PTEN-Ctail were observed 2 hours after the addition of CK2 and GSK3β in our experimental conditions.
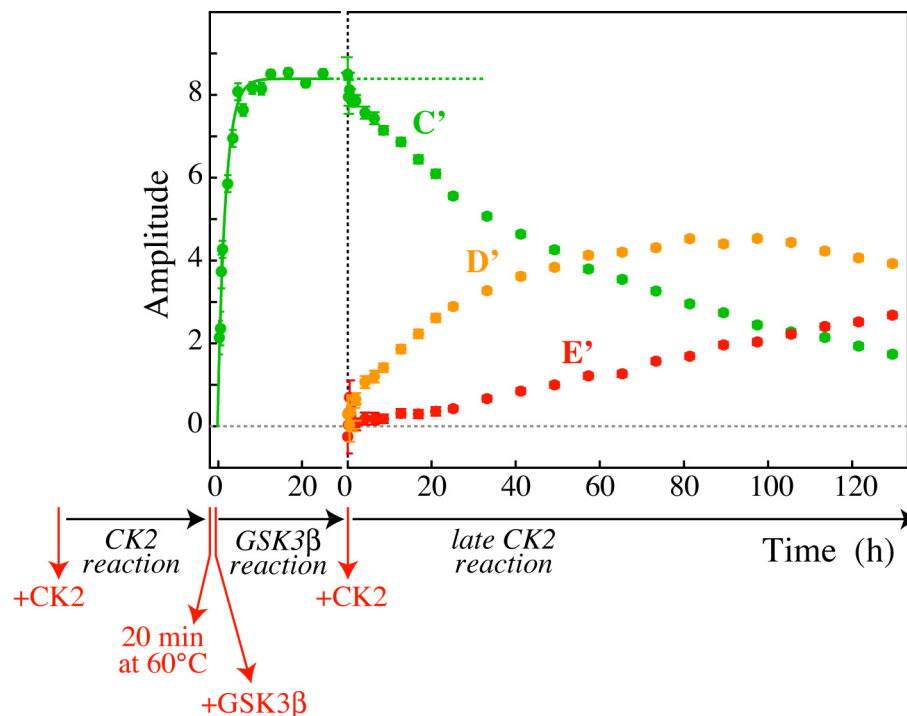
Figure S5. Late phosphorylation of S361 and T363 by CK2. To determine whether S361 and T363 are CK2- or GSK3β-phosphorylation sites, we have performed an experiment consisting in heat-inactivating the CK2 kinase after completion of the CK2 reactions (incubation at 60 °C for 20 min of a sample fully phosphorylated by CK2). A series of ^{1}H-^{15}N HSQC was recorded on this sample after subsequent addition of 10 µl of GSK3β. Since PTEN-Ctail is intrinsically disordered, no substrate denaturation was observed. T366 and S362 were successively phosphorylated by GSK3β. Amplitudes (not normalized) of the average resonance signals for species C' (corresponding to phosphorylated S362^P) are plotted as a function of the GSK3β reaction time (green circles). The amplitude of species C' reaches a stable plateau value indicating that no further phosphorylation on S361 and T363 is controlled by GSK3β. However, adding a new aliquot of CK2 kinase (2 µl) in this sample did induce phosphorylation of these two sites as seen (1) from the disappearance of species C' (green circles) and the concomitant appearance of species D' (phosphorylation of S361, orange circles) and (2) from the disappearance of species D' and appearance of species E' (phosphorylation of T363, red circles). Error bars correspond to the rms of the noise in the corresponding spectrum.
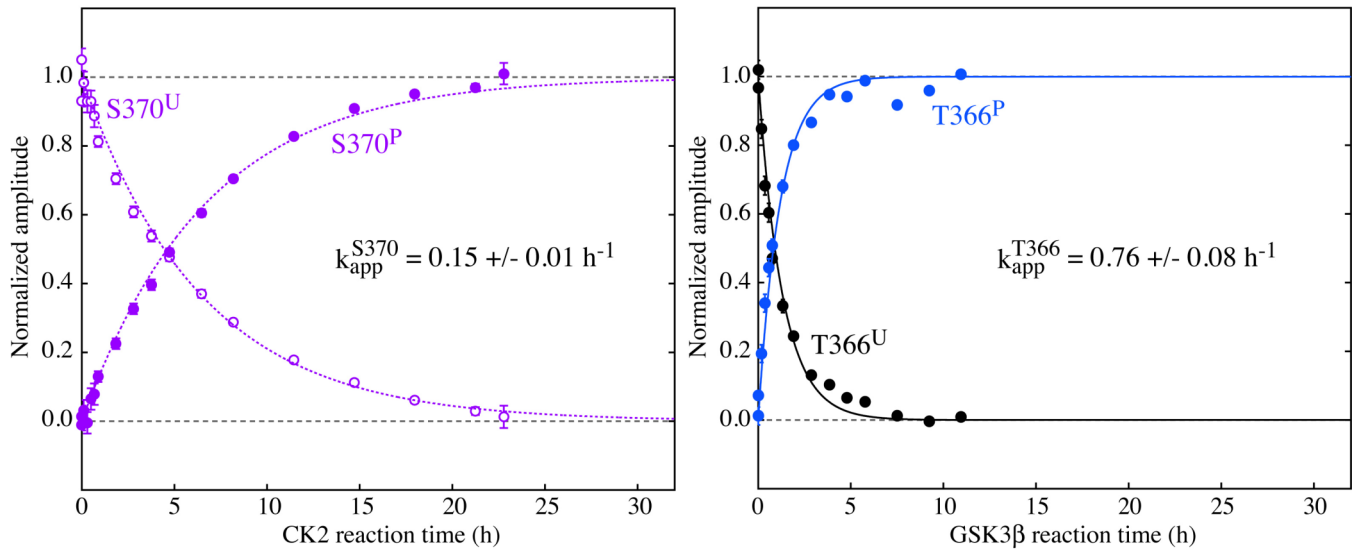
Figure S6. Kinetics of phosphorylation of the quadruple S380A/T382A/T383A/S385A PTEN-Ctail mutant *in vitro*. *Left*: Normalized amplitude of S370^U and S370^P resonances (open and close violet circles) as a function of the CK2-reaction time. The data were fitted to a single exponential function (dashed lines) leading to an apparent rate constant of 0.15 ± 0.01 h^{-1}, identical to that found for the wild type (see main text). *Right*: Normalized amplitude of T366^U and T366^P resonances (black and blue circles) as a function of the GSK3β-reaction time. This indicates that, once S370 is phosphorylated by CK2, the GSK3β-catalyzed cascade proceeds normally as for the wild type. It also indicates that the phosphorylation state within the S380-S385 cluster has no influence on the phosphorylation of S370, i.e., that the cascades initiated on S385 and S370 are independent.
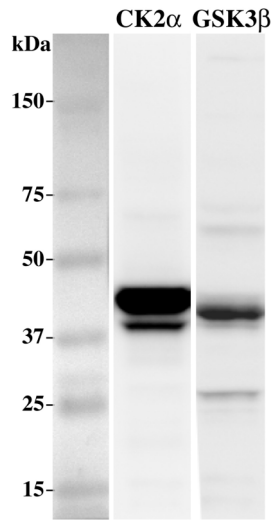
Figure S7. Western Blot. Immunoblots revealing the presence of endogenous CK2α (45 kDa) and

GSK3β (47 kDa) kinases in the SH-SY5Y human neuroblastoma cell extracts.
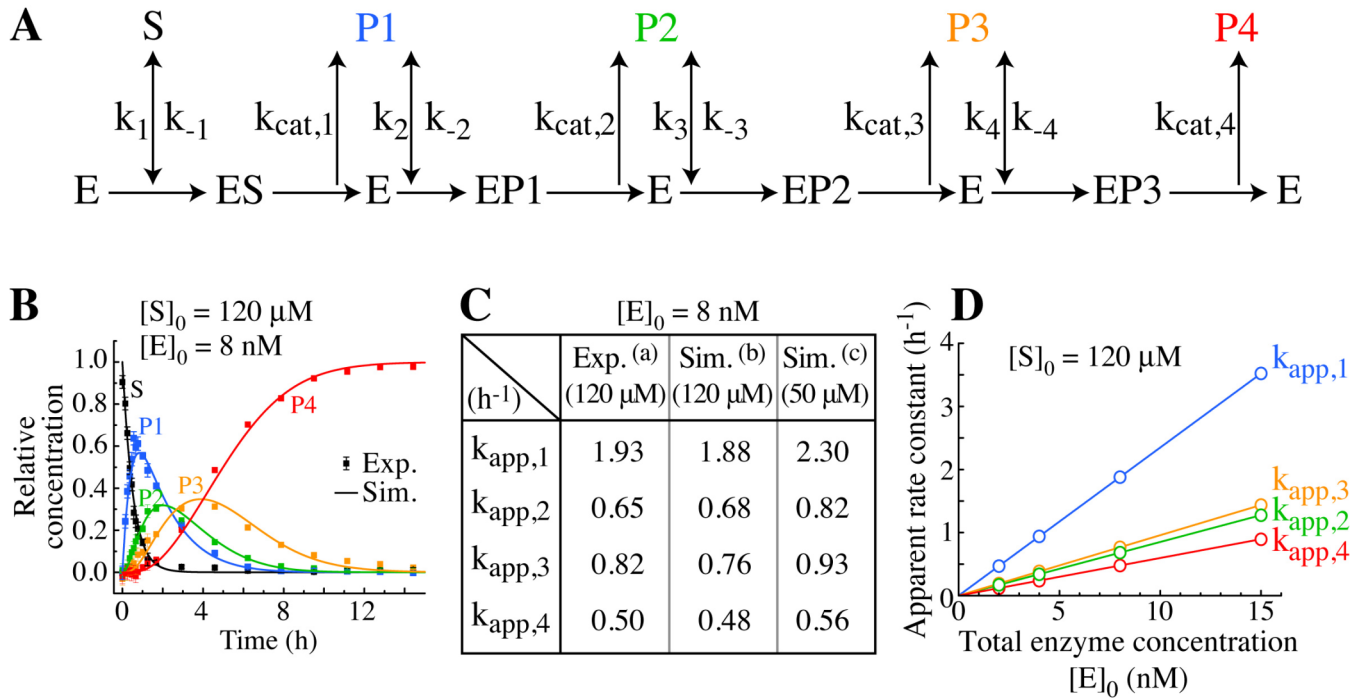

Figure S8. Simulation of the dynamical process of phosphorylation in the S380-S385 cluster. (A).

Sequential oversimplified enzymatic reaction model in the S380-S385 cluster. E is the enzyme, S is the

unphosphorylated substrate, P1, P2 and P3 are the three released intermediate products with 1, 2 and 3

phosphorylated sites and P4 is the fully phosphorylated product (S, P1 to P4 correspond to species A, B to E in our model described by equation (1) of the manuscript). ES, EP1 to EP3 are the enzyme/substrate complexes transiently formed during the chain reaction. k_i and k_{-i} are the rates for reversible enzyme binding and $k_{cat,i}$ the constant characterizing the overall process leading to catalysis and to dissociation of the phosphorylated product from the enzyme. The sum of the concentrations of substrate in its different states is assumed constant though the reaction, so that $[S]+[P1]+[P2]+[P3]+[P4]$ = $[S]_0$, $[S]_0$ being the initial substrate concentration (the concentration of the bound species ES, EP1 to EP3 are neglected). The concentration of enzyme, $[E]_0$, is constant though the reaction. **(B)** The simulation of the variation of the concentration of substrate and product in the time course of the reaction is shown as lines (in black, blue, green, orange and red for S, P1, P2, P3 and P4, respectively), using the optimized set of k_i, k_{-i} and $k_{cat,i}$ parameters (see Materials and Methods of Supporting Information above) and our experimental conditions: $[S]_0$ = 120 μM and $[E]_0$ = 8 nM. The NMR experimental data are shown as filled squares (with the same color-coding for species A, B, C, D and E, respectively). **(C)** Influence of the initial substrate concentration on the apparent rate constants. Table of the apparent rate constants $k_{app,1}$, $k_{app,2}$, $k_{app,3}$ and $k_{app,4}$ (in h^{-1}) extracted from fitting (a) our experimental data recorded at $[S]_0$ = 120 μM, (b) the simulated data performed at $[S]_0$ = 120 μM and (c) the simulated data performed at $[S]_0$ = 50 μM (at constant $[E]_0$ = 8 nM). **(D)** Influence of the enzyme concentration on the apparent rate constants. Plot of the apparent rate constants $k_{app,1}$, $k_{app,2}$, $k_{app,3}$ and $k_{app,4}$ (blue, green, orange and red, respectively) extracted from fitting the simulated data performed at various enzyme concentrations $[E]_0$ (at constant $[S]_0$ = 120 μM). The solid line corresponds to linear regression.

Tables

Table S1. Values of the apparent rate constants (h^{-1}) of the phosphorylation reactions within the S380-S385 cluster.

Species	$k_{app,1}$ (S385) (h^{-1})	$k_{app,2}$ (S380) (h^{-1})	$k_{app,3}$ (T383) (h^{-1})	$k_{app,4}$ (T382) (h^{-1})
A [1]	**1.93 ± 0.29**	NA	NA	NA
B [1]	1.93 [2]	**0.65 ± 0.01**	NA	NA
	2.15 ± 0.32	0.64 ± 0.002	NA	NA
C [1]	1.93 [2]	0.65 [3]	**0.82 ± 0.05**	NA
	1.93 [2]	0.64 ± 0.05	0.82 ± 0.05	NA
D [1]	1.93 [2]	0.65 [3]	0.82 [4]	**0.49 ± 0.04**
	1.93 [2]	0.65 [3]	0.85 ± 0.11	0.49 ± 0.04
E [1]	1.93 [2]	0.65 [3]	0.82 [4]	**0.51 ± 0.04**
	1.93 [2]	0.65 [3]	0.99 ± 0.30	0.48 ± 0.09
A+B [1]	1.93 [2]	0.64 ± 0.09	NA	NA
B+C [1]	1.93 [2]	0.65 [3]	0.77 ± 0.02	NA
C+D [1]	1.93 [2]	0.65 [3]	0.82 [4]	0.58 ± 0.01
C+D+E [1]	1.93 [2]	0.65 [3]	0.82 [4]	0.84 ± 0.03 [6]
D+E [1]	1.93 [2]	0.65 [3]	0.82 [4]	0.65 ± 0.02
Global A to E [5]	2.00 ± 0.05	0.65 ± 0.01	0.83 ± 0.02	0.49 ± 0.06
Consensus values	**1.93 ± 0.29**	**0.65 ± 0.01**	**0.82 ± 0.05**	**0.50 ± 0.04**

[1] Values of the apparent rate constants correspond to averages and standard deviations over individual fits of each representative of a phosphorylated species (or combinations of species) as indicated in Supporting Figure S2. These values depend on the concentration of kinase and substrate (8 nM CK2 and 120 µM PTEN-Ctail).

[2] Average $k_{app,1}$ deduced from fitting kinetics of A.

[3] Average $k_{app,2}$ deduced from fitting kinetics of B.

[4] Average $k_{app,3}$ deduced from fitting kinetics of C.

[5] Global fit of average of species A, B, C, D, E. Errors correspond to standard errors (from Monte Carlo analysis).

[6] Since C+D+E = 1-A-B, this combination of species is essentially dependant on $k_{app,1}$ and $k_{app,2}$. Thus, the value of $k_{app,4}$ cannot be inferred from such a combination.

Table S2. Values of the apparent rate constants (h^{-1}) of the isolated phosphorylation S370.

	k_{app} (S370) (h^{-1})
U [1]	0.16 ± 0.01
P [1]	0.15 ± 0.01
Consensus values [2]	**0.15 ± 0.01**

[1] Values of the apparent rate constants correspond to averages and standard deviations over individual fits performed on each representative of the unphosphorylated (U) or phosphorylated (P) species. Representative residues of the phosphorylation of S370 were S370$^{U/P}$, V369, N372. These values depend on the concentration of kinase and substrate (8 nM CK2 and 120 µM PTEN-Ctail).

[2] Consensus values correspond to average and standard deviation of fitting the U and P species (the two lines above).

Table S3. Values of the apparent rate constants (h^{-1}) of the phosphorylation reactions within the S361-T366 cluster.

Species	k'$_{app,1}$ (T366) (h^{-1})	k'$_{app,2}$ (S362) (h^{-1})	k'$_{app,3}$ (S361) (h^{-1})	k'$_{app,4}$ (T363) (h^{-1})
A' (T366^U) [1]	0.46 ± 0.01	NA	NA	NA
1 – A' (T366^P) [1]	0.41 ± 0.01	NA	NA	NA
A'+B' [1]	0.43 [2]	**0.193 ± 0.010**	NA	NA
C' [1]	0.43 [2]	0.193 [3]	**0.012 ± 0.001**	NA
D' [1]	0.43 [2]	0.193 [3]	0.012 [4]	**< 0.006 ± 0.001 [5]**
Consensus values	**0.43 ± 0.03**	**0.193 ± 0.010**	**0.012 ± 0.001**	**< 0.006 ± 0.001 [5]**

[1] Values of the apparent rate constants correspond to individual fits of the average amplitudes representative of a species (or a combination of species) as indicated in Figure 3 and standard errors come from Monte Carlo analysis. These values depend on the concentration of kinases and substrate (8 nM CK2, 39 nM GSK3β and 120 µM PTEN-Ctail). For T366^U (species A') and T366^P (species B'+C'+D'+E' = 1 – A') the apparent rate constant was extracted from a fit to single exponential functions.

[2] k'$_{app,1}$ deduced from consensus value of fitting kinetics of A' and 1 – A'.

[3] k'$_{app,2}$ deduced from fitting kinetics of A'+B'.

[4] k'$_{app,3}$ deduced from fitting kinetics of C'.

[5] Poor accuracy on k'$_{app,4}$, since the decay of species D' is not sampled.

References

(1)   Terrien, E.; Simenel, C.; Prehaud, C.; Buc, H.; Delepierre, M.; Lafon, M.; Wolff, N. *Biomol NMR Assign* 2009, *3*, 45-8.

(2)   Prehaud, C.; Wolff, N.; Terrien, E.; Lafage, M.; Megret, F.; Babault, N.; Cordier, F.; Tan, G. S.; Maitrepierre, E.; Menager, P.; Chopy, D.; Hoos, S.; England, P.; Delepierre, M.; Schnell, M. J.; Buc, H.; Lafon, M. *Sci Signal* 2010, *3*, ra5.

(3)   Loh, S. H. Y.; Francescut, L.; Lingor, P.; Bahr, M.; Nicotera, P. *Cell Death and Differentiation* 2008, *15*, 283-298.